

Deviation from the Classical Colloid Filtration Theory in the Presence of Repulsive DLVO Interactions

Nathalie Tufenkji^{*,†} and Menachem Elimelech[‡]

Department of Chemical Engineering, McGill University, Montreal, Quebec H3A 2B2, Canada, and Department of Chemical Engineering, Environmental Engineering Program, P.O. Box 208286, Yale University, New Haven, Connecticut 06520-8286

Received May 31, 2004. In Final Form: September 8, 2004

A growing body of experimental evidence suggests that the deposition behavior of microbial particles (e.g., bacteria and viruses) is inconsistent with the classical colloid filtration theory (CFT). Well-controlled laboratory-scale column deposition experiments were conducted with uniform model particles and collectors to obtain insight into the mechanisms that give rise to the diverging deposition behavior of microorganisms. Both the fluid-phase effluent particle concentration and the profile of retained particles were systematically measured over a broad range of physicochemical conditions. The results indicate that, in the presence of repulsive Derjaguin–Landau–Verwey–Overbeek (DLVO) interactions, the concurrent existence of both favorable and unfavorable colloidal interactions causes significant deviation from the CFT. A dual deposition mode model is presented which considers the combined influence of “fast” and “slow” particle deposition. This model is shown to adequately describe both the spatial distribution of particles in the packed bed and the suspended particle concentration at the column effluent.

Introduction

The classical colloid filtration theory (CFT) is the most commonly used approach for predicting particle deposition behavior in saturated porous media. Originally developed by Yao et al.,¹ this conceptual model is of practical interest in chromatographic separation,² granular (deep-bed) filtration in water and wastewater treatment,^{3,4} transport and fate of colloids and colloid-associated pollutants in the subsurface environment,^{5–7} and natural filtration of microorganisms such as bacteria, viruses, and protozoa.^{8–10}

In this classic “clean-bed” filtration model, the removal of suspended particles is described by first-order kinetics, resulting in concentrations of suspended and retained particles that decay exponentially with distance. However, a growing body of experimental evidence suggests that the deposition of microbial particles (e.g., bacteria and viruses) is inconsistent with the classical CFT.^{11–17} In most

experiments presented, particle deposition rates decline monotonically with distance. Such observations of microbial deposition which diverge significantly from predictions based on the CFT have important implications for numerous processes in natural and engineered systems. Particularly, these results suggest that predictions of particle removal in saturated porous media are considerably overestimated by the classical CFT. Several explanations have been proposed to account for this observed deviation from the CFT, including heterogeneity in microbial surface properties,^{12,17} distributions in the interaction energies between microorganisms and collector grains,¹⁸ and particle deposition dynamics.¹⁸ Although the causes of deviation from the CFT with respect to filtration of microbial particles have been hypothesized, the mechanisms controlling this behavior have not been elucidated.

Laboratory-scale column experiments conducted with model uniform particles and collector grains under well-defined physicochemical conditions can provide insight into the mechanisms that give rise to the diverging deposition behavior of microorganisms. However, such controlled studies where the profiles of retained particles are quantified are scarce.^{19–22} Fitzpatrick and Spielman²² measured the fluid-phase concentration profiles of uniform latex particles in columns packed with spherical glass

* Corresponding author. Phone: (514) 398-4494. Fax: (514) 398-6678. E-mail: nathalie.tufenkji@mcgill.ca.

[†] McGill University.

[‡] Yale University.

(1) Yao, K. M.; Habibian, M. T.; O'Melia, C. R. *Environ. Sci. Technol.* **1971**, *5*, 1105–1112.

(2) Prieve, D. C.; Hoysan, P. M. *J. Colloid Interface Sci.* **1978**, *64*, 201–213.

(3) Tobiasson, J. E.; O'Melia, C. R. *J. Am. Water Works Assoc.* **1988**, *80*, 54–64.

(4) Tien, C.; Payatakes, A. C. *AIChE J.* **1979**, *25*, 737–759.

(5) McDowell-Boyer, L. M.; Hunt, J. R.; Sitar, N. *Water Resour. Res.* **1986**, *22*, 1901–1921.

(6) McCarthy, J. F.; Zachara, J. M. *Environ. Sci. Technol.* **1989**, *23*, 496–502.

(7) Ryan, J. N.; Elimelech, M. *Colloids Surf., A* **1996**, *107*, 1–56.

(8) Harvey, R. W.; Garabedian, S. P. *Environ. Sci. Technol.* **1991**, *25*, 178–185.

(9) Schijven, J.; de Bruin, H. A. M.; Hassanzadeh, S. M.; Husman, A. M. D. *Water Res.* **2003**, *37*, 2186–2194.

(10) Tufenkji, N.; Ryan, J. N.; Elimelech, M. *Environ. Sci. Technol.* **2002**, *36*, 422a–428a.

(11) Albinger, O.; Biesemeyer, B. K.; Arnold, R. G.; Logan, B. E. *FEMS Microbiol. Lett.* **1994**, *124*, 321–326.

(12) Baygents, J. C.; Glynn, J. R.; Albinger, O.; Biesemeyer, B. K.; Ogden, K. L.; Arnold, R. G. *Environ. Sci. Technol.* **1998**, *32*, 1596–1603.

(13) Bolster, C. H.; Mills, A. L.; Hornberger, G. M.; Herman, J. S. *Water Resour. Res.* **1999**, *35*, 1797–1807.

(14) Camesano, T. A.; Logan, B. E. *Environ. Sci. Technol.* **1998**, *32*, 1699–1708.

(15) Martin, M. J.; Logan, B. E.; Johnson, W. P.; Jewett, D. G.; Arnold, R. G. *J. Environ. Eng. Div. (Am. Soc. Civ. Eng.)* **1996**, *122*, 407–415.

(16) Redman, J. A.; Estes, M. K.; Grant, S. B. *Colloids Surf., A* **2001**, *191*, 57–70.

(17) Simoni, S. F.; Harms, H.; Bosma, T. N. P.; Zehnder, A. J. B. *Environ. Sci. Technol.* **1998**, *32*, 2100–2105.

(18) Tufenkji, N.; Redman, J. A.; Elimelech, M. *Environ. Sci. Technol.* **2003**, *37*, 616–623.

(19) Li, X.; Scheibe, T. D.; Johnson, W. P. *Environ. Sci. Technol.*, in press.

(20) Bradford, S. A.; Simunek, J.; Bettahar, M.; van Genuchten, M. T.; Yates, S. R. *Environ. Sci. Technol.* **2003**, *37*, 2242–2250.

(21) Bradford, S. A.; Yates, S. R.; Bettahar, M.; Simunek, J. *Water Resour. Res.* **2002**, *38*, 1327–1338.

(22) Fitzpatrick, J. A.; Spielman, L. A. *J. Colloid Interface Sci.* **1973**, *43*, 350–369.

beads by sampling at successive depths of the packed bed using hypodermic needle probes. Under conditions where electrostatic double-layer repulsion is not important, deposition rates determined from the slope of the particle concentration profile were in good agreement with theoretical predictions.^{22,23} Bradford et al.^{20,21} observed that the spatial distributions of latex colloids in columns packed with glass beads and Ottawa sand were not well described by the classical CFT. In their studies, however, physical straining was believed to be a significant particle removal mechanism. Since the contribution of straining to particle removal is not considered in the CFT, the work of Bradford et al. is not appropriate in determining the causes of deviation from the CFT.

In this paper, we present well-controlled laboratory-scale column deposition experiments to investigate the mechanisms and causes of deviation from the CFT. Emphasis was placed on conditions where repulsive electrostatic double-layer interactions predominate. Uniform polystyrene latex colloids and spherical soda-lime glass beads were selected as model particles and collectors, respectively. To examine the validity of the classical CFT, we systematically measured both the fluid-phase effluent particle concentration and the profile of retained particles over a broad range of physicochemical conditions. We demonstrate that the CFT breaks down in the presence of repulsive electrostatic interactions. A dual deposition mode model is applied which considers the simultaneous "fast" and "slow" deposition of colloids. This model is shown to adequately describe both the spatial distribution of particles in the packed bed and the suspended particle concentration at the column effluent.

Theory

Classical Colloid Filtration Theory. The transport of colloidal particles through saturated homogeneous porous media can be described by accounting for particle advection, hydrodynamic dispersion, and deposition (filtration). For relatively low particle concentration and moderate ionic strength, blocking and ripening effects are not significant and particle release is typically negligible. Under these conditions, the concentrations of fluid-phase particles, $C(x, t)$, and retained particles, $S(x, t)$, at column depth x and time t can be described by a one-dimensional advection–dispersion equation with a first-order kinetic deposition term:^{24,25}

$$\frac{\partial C}{\partial t} + \frac{\rho_b}{\epsilon} \frac{\partial S}{\partial t} = D \frac{\partial^2 C}{\partial x^2} - v \frac{\partial C}{\partial x} \quad (1)$$

$$\frac{\rho_b}{\epsilon} \frac{\partial S}{\partial t} = kC \quad (2)$$

Here, v is the interstitial particle velocity, D is the hydrodynamic dispersion coefficient, ϵ is the bed porosity, ρ_b is the porous medium bulk density, and k is the particle deposition rate coefficient. The latter is related to the commonly used single-collector removal efficiency, η ,^{1,24,26} via

(23) Spielman, L. A.; Fitzpatrick, J. A. *J. Colloid Interface Sci.* **1973**, *42*, 607–623.

(24) Grolimund, D.; Elimelech, M.; Borkovec, M.; Barmettler, K.; Kretzschmar, R.; Sticher, H. *Environ. Sci. Technol.* **1998**, *32*, 3562–3569.

(25) Kretzschmar, R.; Barmettler, K.; Grolimund, D.; Yan, Y. D.; Borkovec, M.; Sticher, H. *Water Resour. Res.* **1997**, *33*, 1129–1137.

(26) Tufenkji, N.; Elimelech, M. *Environ. Sci. Technol.* **2004**, *38*, 529–536.

$$k = \frac{3(1 - \epsilon)v}{2d_c} \eta \quad (3)$$

where d_c is the diameter of the collector grains.

For most applications of practical interest (e.g., chromatographic separation and granular filtration), the system is considered at steady state and the influence of hydrodynamic dispersion is negligible. It is also typically assumed that the rate of particle deposition is both spatially and temporally invariant; that is, a single value of k is specified. Under these conditions, for a continuous particle injection at concentration C_0 (at $x = 0$) and time period t_0 , the solutions to eqs 1 and 2 for a column initially free of particles are

$$C(x) = C_0 \exp\left[-\frac{k}{v}x\right] \quad (4)$$

$$S(x) = \frac{t_0 \epsilon k}{\rho_b} C(x) = \frac{t_0 \epsilon k C_0}{\rho_b} \exp\left[-\frac{k}{v}x\right] \quad (5)$$

Equation 4 is commonly referred to as the classical colloid filtration model and has been used extensively in modeling the transport of model colloids and microorganisms in saturated porous media.^{8,11,16,25,27,28}

Dual Deposition Mode Model. As discussed previously, the classical CFT is based on the assumption that the particle deposition rate coefficient, k , is constant. However, variability in the colloidal interactions between particles and collector grains can give rise to a distribution in the deposition rate. Particularly, in the presence of repulsive electrostatic double-layer interactions, particles may exhibit a dual deposition mode whereby a fraction of the particle population experiences a fast deposition rate and the remaining particles deposit at a slow rate. The causes of this variation in the particle deposition rate will be discussed in more detail later in the paper. In brief, these fast and slow deposition rates can be attributed to the concurrent existence of both *favorable* and *unfavorable* chemical–colloidal interactions, respectively. Particle deposition is termed *favorable* in the absence of repulsive interaction energies, whereas *unfavorable* deposition refers to the case where repulsive colloidal interactions predominate.²⁸ The occurrence of both *favorable* and *unfavorable* conditions in an otherwise homogeneous system can be considered by including a bimodal distribution of k in the classical colloid filtration theory:¹⁸

$$C(x) = C_0 \int_0^\infty \exp\left[-\frac{k}{v}x\right] p(k) dk \quad (6)$$

$$S(x) = \frac{\epsilon t_0 C_0}{\rho_b} \int_0^\infty k \exp\left[-\frac{k}{v}x\right] p(k) dk \quad (7)$$

where $p(k)$ is the linear combination of two normal (Gaussian) distributions:

$$p(k) = f_{\text{slow}} \frac{1}{\sigma_{\text{slow}} \sqrt{2\pi}} \exp\left[-\frac{1}{2} \left(\frac{k - \bar{k}_{\text{slow}}}{\sigma_{\text{slow}}}\right)^2\right] + f_{\text{fast}} \frac{1}{\sigma_{\text{fast}} \sqrt{2\pi}} \exp\left[-\frac{1}{2} \left(\frac{k - \bar{k}_{\text{fast}}}{\sigma_{\text{fast}}}\right)^2\right] \quad (8)$$

(27) Martin, R. E.; Bouwer, E. J.; Hanna, L. M. *Environ. Sci. Technol.* **1992**, *26*, 1053–1058.

(28) Elimelech, M.; O'Melia, C. R. *Environ. Sci. Technol.* **1990**, *24*, 1528–1536.

Here, \bar{k}_{slow} and \bar{k}_{fast} are the mean deposition rate coefficients, σ_{slow} and σ_{fast} are the corresponding standard deviations, and f_{slow} and f_{fast} are the fractions of the total population associated with each mode.

Materials and Methods

Colloidal Particles. Surfactant-free fluorescent polystyrene latex colloids (EX 490 nm, EM 515 nm, Interfacial Dynamics Corporation, Portland, OR) with carboxyl-modified functional groups were used as model particles. The monodispersed particles have a mean diameter of $3.0 \mu\text{m}$ and a titrated surface charge density of $119.8 \mu\text{C}/\text{cm}^2$. The density of the particles, as reported by the manufacturer, is $1.055 \text{ g}/\text{cm}^3$.

Porous Media. Spherical soda-lime glass beads (Class V, MO-SCI Corporation, Rolla, MO) were utilized as model collector grains. The manufacturer reported the average diameter of the glass beads as 0.328 mm . The chemical composition (by weight) of the beads is as follows: $\sim 70\%$ SiO_2 , $\sim 3\%$ Al_2O_3 , $\sim 10\%$ CaO , $\sim 3\%$ MgO , $\sim 15\%$ Na_2O , and $<0.3\%$ Fe_2O_3 . The glass beads were thoroughly cleaned to remove grease and other impurities. The beads were soaked in a surfactant solution (2% Extran MA02, EM Science, Gibbstown, NJ) for 1 h, rinsed with deionized (DI) water (Barnstead), sonicated (Aquasonic 150T, VWR Scientific Products, West Chester, PA) for 15 min in a detergent solution (2% RBS 35, Pierce Biotechnology Inc., Rockford, IL), rinsed with DI water, soaked for 24 h in a solution containing sulfuric acid and NOCHROMIX (Godax Laboratories, Inc., Takoma Park, MD), and finally rinsed with DI water until the measured pH reached a value of ~ 5.6 . Clean glass beads were dried in an oven at 100°C . Prior to packing the column, clean glass beads were rehydrated by boiling them in DI water for 30 min. This extensive cleaning procedure yielded very reproducible particle deposition results.

Solution Chemistry. Analytical reagent-grade KCl (Fisher Scientific) and DI water were used to prepare electrolyte solutions. Salt concentrations were varied over a wide range of ionic strengths (3–300 mM) so that *favorable* and *unfavorable* deposition could be studied. The pH of the suspensions was adjusted to 8 by the addition of KHCO_3 (1 mM).

Electrokinetic Characterization of Particles and Collectors. Microelectrophoresis (Zeta-PALS, Brookhaven Instruments Corporation, Holtsville, NY) was used to characterize the electrokinetic properties of the latex particles over the range of ionic strengths used in the column experiments. Electrophoretic mobility was measured at 25°C ($\pm 1^\circ\text{C}$) using particle suspensions (4.7×10^5 particles/mL) prepared in the background electrolyte of interest. ζ -Potentials were calculated from the measured electrophoretic mobilities using the Smoluchowski equation.²⁹

To determine the electrokinetic properties of the porous medium over the range of solution conditions used in the column experiments, 7 g of clean soda-lime glass beads was sonicated (Aquasonic 150T, VWR Scientific Products, West Chester, PA) for 20 min in 12 mL of the electrolyte solution of interest. Following sonication, samples of the supernatant were diluted 10-fold in the background electrolyte solution and electrophoretic mobility measurements taken as described previously (Zeta-PALS, Brookhaven Instruments Corporation, Holtsville, NY). ζ -Potentials were calculated from the measured electrophoretic mobilities using the Smoluchowski equation.²⁹

Deposition Experiments. Transport experiments were conducted by pumping a suspension of latex particles through a glass chromatography column packed with clean soda-lime glass beads. An adjustable-height column (C 16/20, Amersham Biosciences, Piscataway, NJ) with an inner diameter of 1.6 cm was used. The soda-lime glass beads were wet-packed to a height of 12.6 cm with vibration to minimize any layering or air entrapment. Standard gravimetric methods were used to determine the glass bead density ($2.43 \text{ g}/\text{cm}^3$) and a column packing porosity of 0.37.

Prior to each experiment, the packed column was equilibrated by pumping (model 200 syringe pump, KD Scientific Inc., New

Hope, PA) 20 pore volumes of the background electrolyte solution through the column at a constant approach (superficial) velocity of $8.3 \times 10^{-3} \text{ cm}/\text{s}$. A suspension of latex colloids of the same background electrolyte composition was pumped for 2.8 pore volumes followed by a particle-free background electrolyte solution (2.8 pore volumes). A constant influent particle concentration, C_0 , was maintained by including a miniature magnetic stir bar in the particle solution syringe. The particle concentration at the column outlet was monitored on-line using optical density measurements (at 360 nm) with a UV–visible spectrophotometer (Hewlett-Packard model 8453) and a 1 cm flow-through cell. The influent particle concentration was varied between experiments to obtain optimal resolution; specifically, we used $C_0 = 1.7 \times 10^7$ particles/mL for experiments at lower ionic strengths (3, 10, and 30 mM) and $C_0 = 5.4 \times 10^6$ particles/mL for experiments conducted at higher ionic strengths (100 and 300 mM). The total amount of retained particles, N_{dep} , was determined by calculating the difference between the number of particles injected into the column, N_{inj} , and the amount obtained by numerically integrating the particle breakthrough curve, N_{eff} .

In certain experiments, two additional pulses of particle-free electrolyte solutions were pumped through the column to initiate the elution (release) of previously deposited particles. A pulse of 3.2 pore volumes low ionic strength solution (0.1 mM KHCO_3) was first pumped through the column, followed by 2.8 pore volumes of a pH 11 solution (1 mM KOH). The total number of particles released, N_{rel} , was calculated by numerically integrating the two elution pulses, to determine the fraction of released particles, f_{rel} , where $f_{\text{rel}} = N_{\text{rel}}/N_{\text{dep}}$.

Column Dissection and Enumeration of Retained Particles. After completing a colloid deposition experiment, the packed bed was dissected into sections to obtain the spatial distribution of particles in the column. The bottom end-piece was removed without disturbing the packed bed, and the porous medium was extruded in 1 cm wide sections by gravity. The packed bed remained saturated with electrolyte solution during the entire extrusion process so as not to shift or cause release of retained colloids. Each 1 cm section of porous media was placed into a 50 mL polypropylene conical tube containing 5 mL of 1 mM NaOH. In this low ionic strength, high pH (~ 11) solution, the surfaces of both the soda-lime glass beads and the latex colloids are highly negatively charged, causing release of retained colloids from the glass surface. After 1 h, the tubes containing the glass bead–colloid solution mixture were vigorously shaken and vortexed to obtain a homogeneous concentration of latex particles in the supernatant. Representative 1 mL samples of the supernatant from each conical tube were filtered (1225 Sampling Manifold, Millipore, Billerica, MA) with vacuum assistance onto 25 mm diameter polycarbonate membranes (0.22 μm average pore diameter) (Osmonics Inc., Minnetonka, MN). Particle concentrations were determined using an epifluorescent microscope (EX 490 nm, EM 515 nm; BX41, Olympus America, NY) by counting at least 20 fields of view on each membrane. The remaining glass bead–colloid solution mixture in each conical tube was emptied into preweighed aluminum dishes, weighed, and placed in an oven to evaporate the remaining liquid. The mass of glass beads and the volume of solution in each section (i.e., conical tube) were determined by mass balance from the weights of empty dishes, liquid- and bead-filled dishes, dry bead-filled dishes, and the volume sampled for enumeration.

In each experiment, the mass balance of latex particles was determined by comparing the number of deposited particles calculated from integrating the particle breakthrough curve, N_{dep} , to the amount retained on the basis of enumeration in the fluorescent microscope (i.e., $S(x)$). In general, the mass balance was found to be within $\pm 15\%$, but in most experiments, the mass balance was $\pm 9\%$.

Determination of Attachment (Collision) Efficiency. To investigate the role of colloidal interactions on the deviation from the CFT, the particle deposition experiments described above were analyzed in terms of the attachment (collision) efficiency, α .^{1,24,30} Note that the attachment efficiency is the inverse of the

(29) Hunter, R. J. *Foundations of Colloid Science*; Oxford University Press: New York, 2001.

(30) Tobiason, J. E. Ph.D. Dissertation, The Johns Hopkins University, 1987.

Table 1. Electrokinetic Properties of Particles and Collectors and Experimentally Determined Attachment Efficiencies

ionic strength (mM)	ζ -potential (mV)		attachment efficiency ^a			deviation ratio	
	particle	glass beads	α_{BTC}	α_{INT}	α_{SLOPE}	$\alpha_{INT}/\alpha_{BTC}$	$\alpha_{SLOPE}/\alpha_{BTC}$
3	-80.3	-55.2	0.019	0.04	0.90	2.1	47
10	-60.5	-50.2	0.032	0.043	0.74	1.3	23
30	-45.3	-36.6	0.13	0.21	0.53	1.6	4.1
100	-30.1	-18.9	0.31	0.48	0.73	1.5	2.4
300	-27.9	-15.7	0.68	0.65	0.75	0.96	1.1

^a The value of the single-collector contact efficiency ($\eta_0 = 7.9 \times 10^{-3}$) was calculated using eq 9 and the following parameter values: $d_p = 3 \mu\text{m}$, $d_c = 328 \mu\text{m}$, $U = 8.3 \times 10^{-5} \text{ m/s}$, $A = 1 \times 10^{-20} \text{ J}$, $T = 293 \text{ K}$, $\rho_p = 1055 \text{ kg/m}^3$, $\rho_f = 1000 \text{ kg/m}^3$, $\mu = 1.005 \times 10^{-3} \text{ kg/(m s)}$, and $\epsilon = 0.37$.

stability ratio, W , commonly used in coagulation studies. The attachment efficiency is defined as the ratio of the experimental single-collector removal efficiency, η , and the predicted single-collector contact efficiency, η_0 , evaluated from solution of the convective-diffusion equation in the absence of repulsive interaction energies, i.e., $\alpha = \eta/\eta_0$.^{1,26,28} The value of η_0 for the described experimental conditions was determined using a newly developed correlation based on a rigorous numerical solution of the convective-diffusion equation:²⁶

$$\eta_0 = 2.4A_S^{1/3} N_R^{-0.081} N_{Pe}^{-0.715} N_{vdW}^{0.052} + 0.55A_S N_R^{1.675} N_A^{0.125} + 0.22N_R^{-0.24} N_G^{1.11} N_{vdW}^{0.053} \quad (9)$$

where N_R is an aspect ratio, N_{Pe} is the Peclet number, N_A is the attraction number, N_{vdW} is the van der Waals number, and N_G is the gravity number.

Substituting eq 3 into eq 4 and considering the normalized column effluent concentration, $C/C_0|_{x=L}$, at the initial stages of deposition, we obtain the following relationship for the experimental single-collector removal efficiency based on the particle breakthrough curve, η_{BTC} :

$$\eta_{BTC} = -\frac{2}{3} \frac{d_c}{(1-\epsilon)L} \ln(C/C_0) \quad (10)$$

To calculate α_{BTC} for each experiment, the normalized column effluent concentration, C/C_0 , in eq 10 was obtained from each particle breakthrough curve by averaging the values measured between pore volumes 1.8 and 2.

A similar substitution of eq 3 into eq 5 reveals that the single-collector removal efficiency, η , and thus the attachment efficiency, α , can also be obtained from both the prefactor and exponent of the retained profile of particles, $S(x)$. An accurate measure of C_0 in eq 5 was determined by filtering a diluted sample of the influent particle suspension onto a membrane and counting in an epifluorescent microscope as described in the previous section. The value of the attachment efficiency for each experiment was calculated from the intercept, α_{INT} , and slope, α_{SLOPE} , of a semilog plot of the retained particle profile, $S(x)$. More details regarding the calculation of α_{INT} and α_{SLOPE} are provided later in the paper.

Results and Discussion

Electrokinetic Properties of Colloids and Collectors. The ζ -potentials of the latex colloids and soda-lime glass beads as a function of ionic strength are presented in Table 1 (with other parameters to be discussed later). Both the particles and the glass beads are negatively charged at the pH investigated (8), and their ζ -potentials become less negative with increasing ionic strength. Measured ζ -potentials are used later to calculate Derjaguin–Landau–Verwey–Overbeek (DLVO) interaction energy profiles for the latex particle–glass bead system.

Particle Breakthrough Curves. Representative particle breakthrough curves obtained at different solution ionic strengths are presented in Figure 1. In this figure, the normalized effluent particle concentration, C/C_0 , is plotted as a function of time. The results are in qualitative

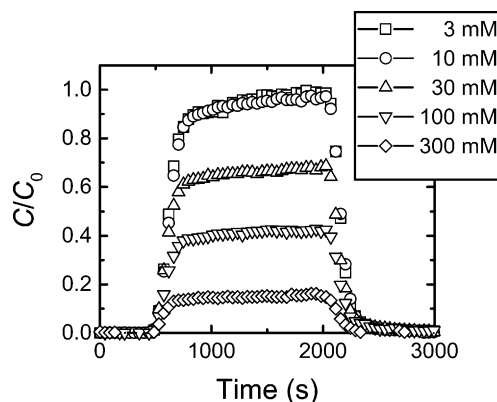


Figure 1. Representative breakthrough curves for experiments conducted with $3.0 \mu\text{m}$ latex particles in columns packed with soda-lime glass beads over a wide range of solution ionic strengths. The key experimental conditions were the following: approach velocity $8.3 \times 10^{-3} \text{ cm/s}$, porosity 0.37, mean bead diameter 0.328 mm , pH 8.0–8.3, and temperature $20\text{--}22 \text{ }^\circ\text{C}$.

agreement with the DLVO theory of colloidal stability.^{31,32} That is, the deposition of latex colloids on the glass beads increases (C/C_0 decreases) with increasing ionic strength. As the concentration of KCl in the solution increases, the diffuse double layers are compressed, causing a reduction in the repulsive electrostatic double-layer forces and an increase in the particle deposition rate.

To study the effect of ionic strength and colloidal interactions on the deviation from the CFT, it is necessary to determine the value of the attachment efficiency, α_{BTC} , from each particle breakthrough curve. As defined previously in the Materials and Methods, the attachment efficiency depends on the colloidal interactions between particles and collectors; it approaches unity when colloidal interactions are favorable for deposition and is much smaller than 1 under unfavorable conditions (i.e., when repulsive interactions predominate). Particle attachment efficiencies, α_{BTC} , were calculated from the normalized effluent particle concentration, C/C_0 , measured in each experiment using eq 10 and the value of η_0 determined from eq 9 ($\alpha = \eta/\eta_0$). Representative results are presented in Table 1 as a function of solution ionic strength (with other parameters to be discussed later). As mentioned earlier, the observed deposition behavior follows the trend predicted by the DLVO theory. An increase in salt concentration from 3 to 300 mM yields an increase in α_{BTC} from 0.019 to 0.68. This large variation in values of the attachment efficiency corresponds to a shift in conditions considered unfavorable for deposition at the lower ionic strengths to completely favorable deposition at the highest

(31) Derjaguin, B. V.; Landau, L. D. *Acta Physicochim. URSS* **1941**, *14*, 733–762.

(32) Verwey, E. J. W.; Overbeek, J. T. G. *Theory of the Stability of Lyophobic Colloids*; Elsevier: Amsterdam, The Netherlands, 1948.

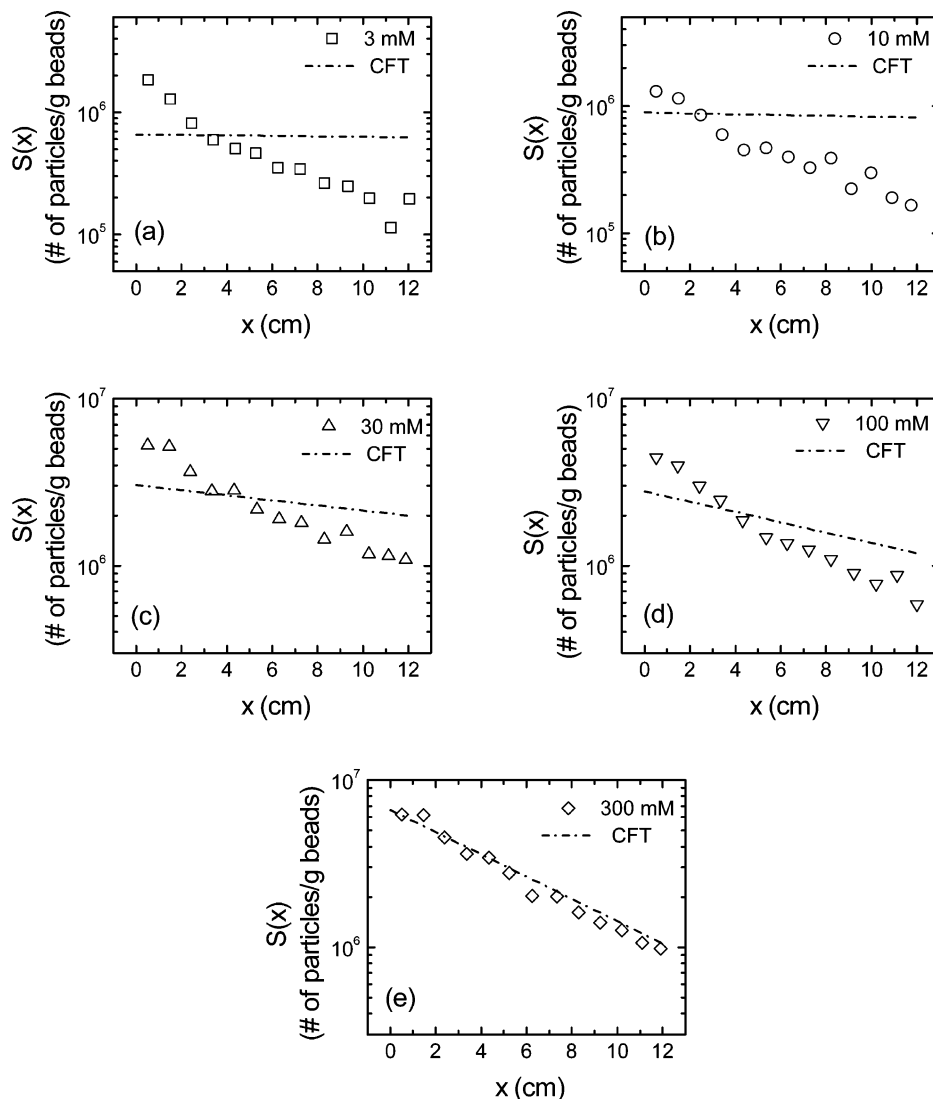


Figure 2. Comparison of experimental retained particle concentration profiles (symbols) and predictions based on the classical CFT using α_{BTC} determined from the corresponding breakthrough curve (dashed lines) for different solution ionic strengths: (a) 3 mM, (b) 10 mM, (c) 30 mM, (d) 100 mM, and (e) 300 mM. Other experimental conditions were the following: approach velocity 8.3×10^{-3} cm/s, porosity 0.37, mean bead diameter 0.328 mm, pH 8.0–8.3, and temperature 20–22 °C.

ionic strength investigated (300 mM). Although several deposition experiments were conducted at each ionic strength, only representative results are presented in Table 1 for purpose of comparison.

Profiles of Retained Particles. The deposition behavior of model colloids in laboratory-scale columns has been examined extensively.^{28,30,33–40} However, studies where the spatial distribution of retained particles in the packed bed has been reported are very scarce. Following the completion of each particle deposition experiment, the spatial distribution of retained particles was determined by carefully dissecting the packed bed. In Figure 2, the profiles of retained particles corresponding

to the breakthrough curves in Figure 1 are presented. The retained particle concentration, $S(x)$, is plotted as a function of distance in a semilog format. For comparison, the profile of retained particles predicted by the CFT (eq 5) using the attachment efficiency determined from the corresponding breakthrough curve, α_{BTC} , is included in each part of Figure 2.

If the classical CFT were valid under these physicochemical conditions, the spatial distribution of particles determined experimentally should correspond exactly to the spatial distribution calculated using eq 5 and values of α_{BTC} . However, inspection of Figure 2 reveals that the measured concentrations are all in marked discrepancy with those predicted by the CFT, with the exception of those measured at 300 mM (Figure 2e). This deviation between profiles of retained particles is particularly evident at the lowest ionic strength investigated (3 mM, Figure 2a). As the salt concentration in the solution increases, the observed spatial distribution of particles approaches that calculated using values of α_{BTC} (Figure 2b–d). At the highest ionic strength considered (300 mM, Figure 2e), the concentrations of retained colloids determined experimentally are in excellent agreement with those predicted by the classical CFT (i.e., using values of

(33) Roy, S. B.; Dzombak, D. A. *Colloids Surf., A* **1996**, *107*, 245–262.

(34) Harmand, B.; Rodier, E.; Sardin, M.; Dodds, J. *Colloids Surf., A* **1996**, *107*, 233–244.

(35) Elimelech, M.; Nagai, M.; Ko, C. H.; Ryan, J. N. *Environ. Sci. Technol.* **2000**, *34*, 2143–2148.

(36) Bai, R.; Tien, C. J. *Colloid Interface Sci.* **1999**, *218*, 488–499.

(37) Franchi, A.; O'Melia, C. R. *Environ. Sci. Technol.* **2003**, *37*, 1122–1129.

(38) McDowell-Boyer, L. M. *Environ. Sci. Technol.* **1992**, *26*, 586–593.

(39) Elimelech, M. *J. Colloid Interface Sci.* **1994**, *164*, 190–199.

(40) Elimelech, M.; O'Melia, C. R. *Langmuir* **1990**, *6*, 1153–1163.

α_{BTC}). Under these solution conditions, the spatial distribution of retained particles in the packed bed clearly exhibits an exponential decay. However, at lower salt concentrations, a characteristic profile of retained particles is observed with two distinct regions: a steeper slope at the top of the column, followed by a flatter, more shallow slope at the bottom. This distinctive feature of the measured profile of retained particles is particularly evident for the experiment conducted at 3 mM (Figure 2a).

To quantify the degree of deviation from the CFT at different solution conditions, the attachment efficiency for each experiment was calculated from the measured profiles of deposited particles, $S(x)$. Linearization of eq 5 reveals that the particle deposition rate coefficient, k , and thus the attachment efficiency, α , can be obtained from both the intercept and the slope of a semilog plot of $S(x)$:

$$\ln S(x) = \ln\left(\frac{t_0 \epsilon C_0}{\rho_b} k\right) - \frac{k}{v} x \quad (11)$$

where $k = \alpha k_{\text{fav}}$ and k_{fav} is related to η_0 via eq 3. Representative values of the particle attachment efficiency calculated from the intercept, α_{INT} , and the slope, α_{SLOPE} , of $S(x)$ are presented in Table 1.

To demonstrate the difference in values of α calculated from either the particle breakthrough curve (α_{BTC}) or the profile of retained particles (α_{INT} and α_{SLOPE}), the following deviation ratios were calculated for each experiment: $\alpha_{\text{INT}}/\alpha_{\text{BTC}}$ and $\alpha_{\text{SLOPE}}/\alpha_{\text{BTC}}$ (Table 1). In such a comparison, a ratio of 1 indicates perfect agreement between the observed spatial distribution of particles and that predicted by the CFT (i.e., $\alpha_{\text{BTC}} = \alpha_{\text{INT}} = \alpha_{\text{SLOPE}}$). As shown in the table, the deviation ratios are approximately equal to 1 at the highest ionic strength investigated (300 mM). The values of these ratios become greater with decreasing ionic strength, indicating an increased digression between the measured and predicted profiles of retained particles. This significant deviation is emphasized in the ratio $\alpha_{\text{SLOPE}}/\alpha_{\text{BTC}}$. At a salt concentration of 3 mM, the attachment efficiency determined from the slope of the retained particle profile, α_{SLOPE} , is 47 times greater than that calculated from the particle breakthrough curve, α_{BTC} . This considerable difference between measured and predicted deposition behavior is particularly surprising in view of the fact that all experiments were conducted in a well-defined system using uniform spherical particles and collectors. Thus, these results suggest that the observed deviation at lower ionic strengths must be attributed to a removal mechanism which is not accounted for in the classical CFT.

It is worthwhile mentioning that additional column experiments were conducted using DI water to maximize the degree of repulsive (*unfavorable*) colloidal interactions on the retention of latex particles. In this type of experiment, any removal in the packed column can be attributed to the influence of a physical mechanism such as straining.⁴¹ The 3 μm particles demonstrated complete breakthrough ($C/C_0 = 1.0$) in DI water, indicating that physical straining does not play a role in the removal of these particles and thus cannot account for the deviation from the CFT observed in this system.

DLVO Interaction Energy Profiles. Attachment efficiencies calculated from both the particle breakthrough curves, α_{BTC} , and the corresponding retained particle

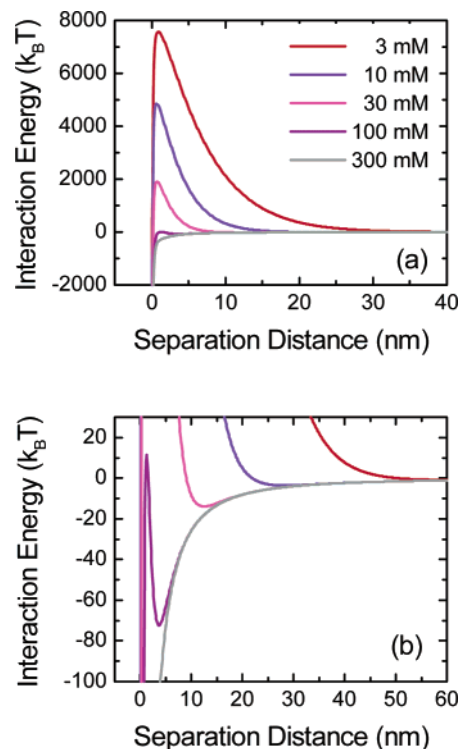


Figure 3. (a) Calculated DLVO interaction energy plotted as a function of separation distance for different solution ionic strengths. (b) Identical data is replotted to highlight the depth and location of the secondary energy minimum. Measured ζ -potentials (Table 1) and a Hamaker constant of 1×10^{-20} J were used to calculate interaction energies.

profiles, α_{INT} and α_{SLOPE} , are not in agreement over the range of solution conditions investigated, except at the highest ionic strength of 300 mM (Table 1). A consistent decrease in the value of the deviation ratio $\alpha_{\text{SLOPE}}/\alpha_{\text{BTC}}$ with increasing salt concentration suggests that colloidal interactions strongly influence the observed particle deposition behavior. To better understand the mechanisms controlling the observed deviation from the classical CFT, the DLVO theory is used to calculate colloidal interaction energies. The DLVO theory considers the sum of London–van der Waals (VDW) attraction and electrostatic double-layer repulsion (EDL). The total interaction energy, namely, the sum of VDW and EDL interactions, was determined by treating the particle–glass bead system as a sphere–plate interaction. Constant-potential EDL interactions were calculated using the expression of Hogg et al.,⁴² where the ζ -potentials of the latex colloids and the soda-lime glass beads were used in place of the respective surface potentials. The retarded VDW attractive interaction energy was calculated from the expression proposed by Gregory.⁴³ A value of 1×10^{-20} J was chosen for the Hamaker constant of the glass–water–polystyrene system.^{3,28,40}

DLVO interaction energy profiles for the latex particle–glass bead system are presented in Figure 3a at the different solution conditions used in the deposition experiments. The calculations reveal the presence of a significant repulsive energy barrier to deposition at nearly all ionic strengths, ranging from 7570 $k_B T$ at 3 mM to 12 $k_B T$ at 100 mM. In contrast, no energy barrier to deposition (i.e., completely *favorable* conditions) is predicted at 300 mM. Hence, on the basis of DLVO interaction energy

(41) Tufenkji, N.; Miller, G. F.; Ryan, J. N.; Harvey, R. W.; Elimelech, M. *Environ. Sci. Technol.*, in press.

(42) Hogg, R.; Healy, T. W.; Fuerstenau, D. W. *Trans. Faraday Soc.* **1966**, *62*, 1638–1651.

(43) Gregory, J. J. *Colloid Interface Sci.* **1981**, *83*, 138–145.

Table 2. Calculated Secondary Minimum Depths and Associated Attachment Efficiencies

ionic strength (mM)	$\Phi_{2^{\circ}\text{min}}^a$ ($k_B T$)	$\alpha_{2\text{min}}^b$
3	0.85	0.36
10	3.6	0.93
30	13.9	1
100	72.4	1

^a Determined from DLVO interaction energy profiles (Figure 3).

^b Calculated using Hahn's model⁵⁰ based on Maxwell's kinetic theory.

calculations, latex colloids are not expected to deposit onto the glass bead surfaces (i.e., overcome the repulsive energy barrier) under these solution conditions (except at 300 mM). Despite these DLVO predictions, however, particle deposition is observed even at the lowest ionic strength examined (e.g., $C/C_0 \approx 0.95$ at 3 mM).

In Figure 3b, where the DLVO interaction energy profiles are replotted on a different scale, we note the presence of a secondary energy well at a greater separation distance than that of the energy barrier. A secondary minimum exists because the EDL interaction decreases exponentially with respect to separation distance, whereas the VDW attraction exhibits a power-law dependency with a slower decay. The depths of the secondary minimum, $\Phi_{2^{\circ}\text{min}}$, for the latex particle–glass bead interaction are listed in Table 2 as a function of ionic strength (with another parameter to be discussed later). DLVO calculations indicate that the magnitude of $\Phi_{2^{\circ}\text{min}}$ increases with salt concentration, from 0.85 $k_B T$ at 3 mM to 72.4 $k_B T$ at 100 mM. Inspection of Figure 3b also reveals that the location of the secondary energy well approaches the collector surface with increasing ionic strength.

Because the average kinetic energy of micrometer-sized particles is on the order of 1 $k_B T$, the calculated values of $\Phi_{2^{\circ}\text{min}}$ suggest that colloids could readily be retained in the secondary energy minimum, even at the lowest ionic strength investigated. Thus, despite the sizable repulsive energy barriers predicted at the lower ionic strengths seemingly preventing particle deposition in the primary energy well, attachment in the secondary energy minimum is very likely. Under certain conditions, in particular at moderate ionic strengths where a deep secondary minimum is located relatively close to the collector surface and the height of the repulsive energy barrier is smaller, it is probable that particles are deposited in both the primary and secondary energy wells.³⁷ This concept will be developed in more detail in the next section.

Dual Deposition Mode Model. In 1979, Marmur⁴⁴ proposed a simple model to compute the stability ratio of combined primary and secondary minimum coagulation. Good agreement between model predictions and experimental data supported his theory that under repulsive electrostatic conditions the value of the stability ratio is controlled by the combined influence of the two modes of coagulation. More recently, Franchi and O'Melia³⁷ suggested that under conditions where the repulsive energy barrier is small a fraction of particles retained in the secondary energy well may “jump” over the energy barrier into the primary energy minimum. The authors proposed that deposition may be viewed as a combination of two collection mechanisms. In this section, we further develop this notion to explain the observed deviation from the classical CFT with respect to the measured profiles of retained particles (Figure 2 and Table 1). The fundamental basis of the proposed dual deposition mode (DDM) model (eqs 6–8) is also described.

Why Dual Deposition? A systematic study of particle deposition conducted under well-controlled experimental conditions revealed that the CFT breaks down in the presence of repulsive electrostatic double-layer interactions. We noted earlier a distinctive feature of the measured profiles of retained particles under these conditions: the slope is steeper at the top of the column and becomes more shallow at the bottom. This observed shape of the retained particle profile is characteristic of a bimodal distribution in the particle deposition rate.¹⁸ That is, a fraction of the particle population exhibits a fast deposition rate (implied by the steep slope at the top of the column), whereas the remaining particles experience a slow deposition rate (denoted by the shallow portion of the retained profile). Because the model experimental system used for this study consisted of uniform latex colloids and clean glass bead collectors, it was expected that a constant particle deposition rate would be observed under all solution conditions. Nonetheless, variations in the particle deposition behavior can arise from a number of sources not accounted for in the classical CFT.

(a) Particles Retained in the Secondary Energy Minimum. Calculated DLVO interaction energy profiles (Figure 3) reveal the presence of a secondary minimum that is particularly deep at moderate to high ionic strengths. Although the role of the secondary energy well has been argued,^{30,45,46} recent experimental and theoretical evidence^{37,47–51} suggests that deposition in the secondary minimum can control particle-transport behavior in saturated porous media. Hahn^{50,52} proposed a simple model for estimating particle collision efficiencies based on deposition in the secondary energy minimum. The Maxwell kinetic theory⁵³ is used to predict the fraction of particles with energies greater than the depth of the secondary energy well, that is, the fraction with sufficient kinetic energy to escape from the secondary minimum.⁵⁰ It follows that the attachment efficiency for deposition in the secondary minimum, $\alpha_{2\text{min}}$, is defined as the probability that a particle does not have sufficient energy to escape from the secondary energy well. Theoretical values of $\alpha_{2\text{min}}$ determined using Hahn's model with calculated values of $\Phi_{2^{\circ}\text{min}}$ are listed in Table 2. On the basis of these results, the latex colloids are expected to exhibit a fast rate of deposition into the secondary energy minimum over the range of solution conditions investigated; that is, $\alpha_{2\text{min}}$ is relatively high at 3 mM and approaches unity at higher ionic strengths. This unhindered or *favorable* condition for particle deposition is depicted schematically in Figure 4a.

(b) Fraction of Particle Population Overcomes Energy Barrier. The classic interpretation of particle deposition (e.g., within the framework of the CFT) has been one of particles overcoming a repulsive energy barrier to reach the primary energy minimum (Figure 4b).

(45) Song, L. F.; Elimelech, M. *J. Chem. Soc., Faraday Trans.* **1993**, 89, 3443–3452.

(46) Elimelech, M. Ph.D. Dissertation, The Johns Hopkins University, 1989.

(47) Litton, G. M.; Olson, T. M. *Colloids Surf., A* **1996**, 107, 273–283.

(48) Hahn, M. W.; Abadzie, D.; O'Melia, C. R. *Environ. Sci. Technol.*, in press.

(49) Redman, J. A.; Walker, S. L.; Elimelech, M. *Environ. Sci. Technol.* **2004**, 38, 1777–1785.

(50) Hahn, M. W.; O'Melia, C. R. *Environ. Sci. Technol.* **2004**, 38, 210–220.

(51) Walker, S. L.; Redman, J. A.; Elimelech, M. *Langmuir* **2004**, 20, 7736–7746.

(52) Hahn, M. W. Ph.D. Dissertation, The Johns Hopkins University, 1994.

(53) Kubo, R. *Rep. Prog. Phys.* **1966**, 29, 255–284.

(44) Marmur, A. *J. Colloid Interface Sci.* **1979**, 72, 41–48.

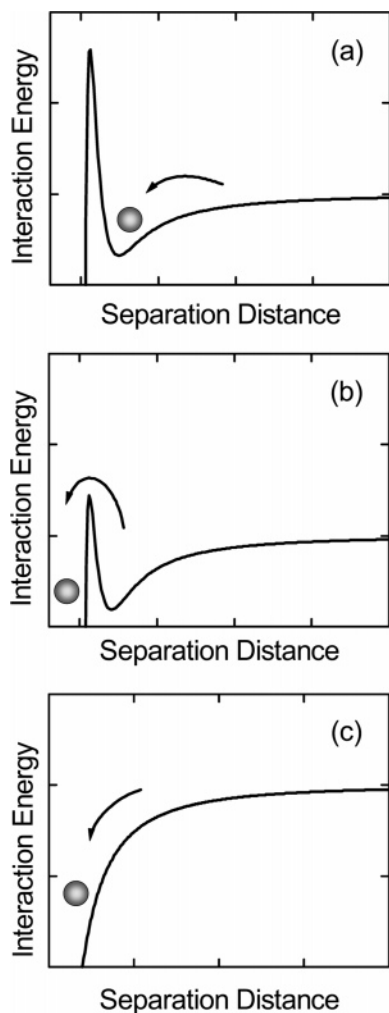


Figure 4. Schematic representations of interaction energy profiles characteristic of (a) particles retained in the secondary energy minimum ($\alpha \approx 1$), (b) particles overcoming the repulsive energy barrier to deposit in the deep primary energy well ($\alpha \ll 1$), and (c) particles depositing on favorable sites owing to the presence of bulk chemical impurities on the collector surface ($\alpha \approx 1$).

However, DLVO calculations presented in Figure 3 indicate the existence of sizable energy barriers to deposition at the lower ionic strengths investigated (3–30 mM). In the calculation of these interaction energy profiles, it was assumed that all particles and collectors have a constant surface potential at a given ionic strength. It has been shown, however, that individual colloidal particles in a suspension may possess different values of surface potentials.^{54,55} This variation in particle surface charge properties gives rise to a distribution in particle–collector interactions, which, in effect, may result in a broader range of colloid deposition rates. Thus, although the calculations presented in Figure 3 predict substantial repulsive energy barriers at the lower ionic strengths examined, variations in particle surface potentials can provide opportunities for a fraction of the particle population to overcome this energy barrier and reach the primary energy well. The presence of a secondary energy minimum can further facilitate this process whereby particles retained in this energy well may jump over the energy barrier into the primary well due to fluctuations in their

internal energy.³⁷ The fraction of the particle population that is able to overcome the repulsive energy barrier and deposit in the primary minimum is referred to as exhibiting a slow deposition rate; that is, the particles are depositing under *unfavorable* conditions. In comparison to those particles which are retained in the secondary energy minimum, a much lower value of the attachment efficiency (i.e., $\alpha \ll 1$) is associated with the fraction of particles which overcomes the repulsive energy barrier.

(c) Surface Charge Heterogeneities Provide Sites for Fast Deposition. A growing body of evidence suggests that the degree of surface charge heterogeneity on particle and/or collector surfaces can control particle deposition behavior under conditions deemed *unfavorable* for deposition.^{56–58} Song et al.⁵⁸ demonstrated that measured particle deposition rates^{40,57} which are considerably greater than those predicted by the DLVO theory could be attributed to the occurrence of bulk and/or surface-bound chemical impurities on the collector surface. In these studies, the bulk chemical impurities in the glass bead collectors consisted of trace amounts of metal oxides, whereas the surface-bound impurities were most likely organic contaminants.^{40,57,58} The glass bead collectors used in the experiments of Litton and Olson⁵⁷ and Elimelech and O'Melia⁴⁰ were similar to those used in the present study. As described previously in the Materials and Methods, the glass beads were composed mainly of SiO₂, but the presence of various metal oxides (Al₂O₃, CaO, MgO, Na₂O, and Fe₂O₃) on the glass bead surface is also worth noting. At the solution pH maintained during experimentation (~8), the metal oxides will be near-neutrally charged or carry a slightly positive charge in comparison to the bulk SiO₂ surface which will be highly negatively charged. Hence, these surface charge heterogeneities are expected to provide *favorable* deposition sites on what is otherwise an *unfavorable* surface for deposition.⁵⁸ Particle deposition under these conditions (i.e., in the absence of a repulsive energy barrier) is characterized by an attachment efficiency of 1 (Figure 4c). It is worthwhile to mention that the degree of surface-bound organic contaminants should not be significant in this study due to the extensive cleaning procedure applied to the glass beads which included the use of a strong oxidizing agent (sulfuric acid with NOCHROMIX).

In this section, we described how the presence of a deep secondary energy minimum as well as metal oxide impurities on the collector surface can provide conditions for *favorable* or fast particle deposition, namely, $\alpha \approx 1$ (Figure 4a and c). In contrast, the general occurrence of repulsive energy barriers gives rise to particle deposition rates which are much slower, exemplified by smaller values of the attachment efficiency, that is, $\alpha \ll 1$ (Figure 4b). This concurrent existence of both *favorable* and *unfavorable* colloidal interactions in an otherwise homogeneous system can be described by considering a bimodal distribution of the particle deposition rate. In the Theory section, a dual deposition mode (DDM) model was presented which incorporates a bimodal distribution of k in the classical colloid filtration theory. The DDM model accounts for the influence of *favorable* deposition sites (where the mean particle deposition rate coefficient is \bar{k}_{fast}) as well as the fraction of particles which deposit at a

(54) Rajagopalan, R.; Chu, R. Q. *J. Colloid Interface Sci.* **1982**, *86*, 299–317.

(55) Dong, H. *J. Microbiol. Methods* **2002**, *51*, 83–93.

(56) Litton, G. M.; Olson, T. M. *J. Colloid Interface Sci.* **1994**, *165*, 522–525.

(57) Litton, G. M.; Olson, T. M. *Environ. Sci. Technol.* **1993**, *27*, 185–193.

(58) Song, L. F.; Johnson, P. R.; Elimelech, M. *Environ. Sci. Technol.* **1994**, *28*, 1164–1171.

Table 3. Comparison of Calculated Dual Deposition Mode (DDM) Model Parameters and Experimental Results

ionic strength (mM)	DDM model parameters and predictions					experimental results	
	$\bar{\alpha}_{fast}^a$	$\bar{\alpha}_{slow}^b$	f_{fast}^b	$C/C_{0 x=L}^c$	R_{adj}^2	f_{rel}^d	$C/C_{0 x=L}$
3	0.87	0.001	0.05	0.95	0.89	NM ^e	0.95
10	0.87	0.003	0.06	0.94	0.94	0.13	0.91
30	0.87	0.04	0.31	0.65	0.96	0.30	0.64
100	0.87	0.04	0.61	0.41	0.98	0.62	0.41

^a Calculated from $\alpha_{max} = 1$, where $\alpha_{max} = \bar{\alpha}_{fast} + 3(0.05)\bar{\alpha}_{fast}$. ^b Determined by nonlinear regression of eq 7 to measured profile of retained particles. Note, $f_{fast} = 1 - f_{slow}$. ^c Predicted by the DDM model. ^d Determined by integration of elution peaks. ^e Not measured.

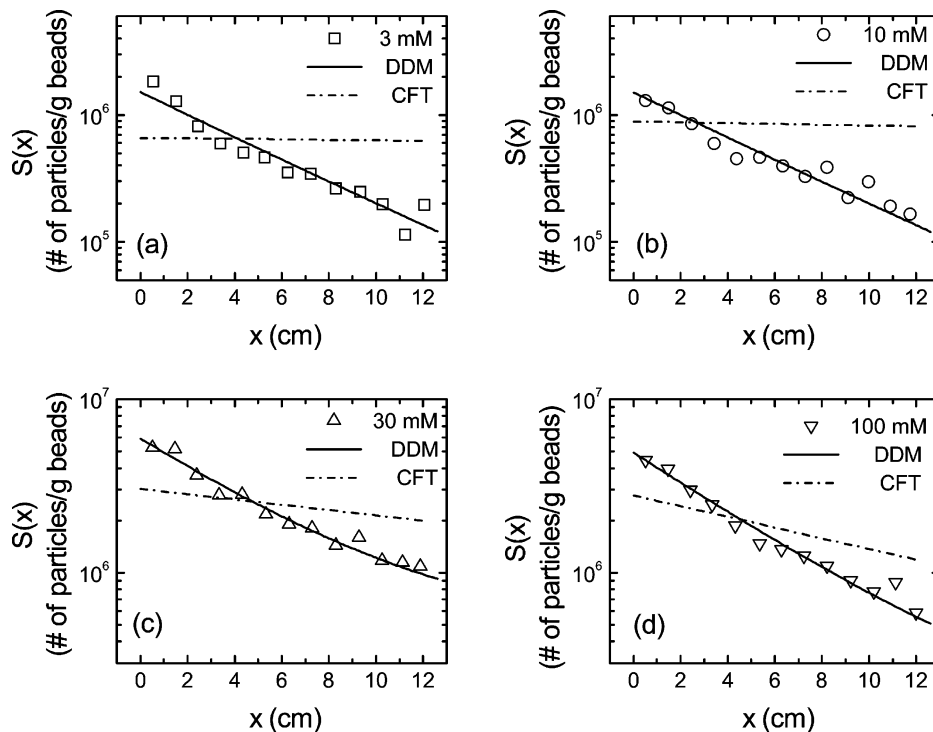


Figure 5. Comparison of experimental retained particle concentration profiles (symbols) and predictions based on the proposed DDM model with two fitting parameters (solid lines) and the classical CFT using α_{BTC} determined from the corresponding breakthrough curve (dashed lines) for different solution ionic strengths: (a) 3 mM, (b) 10 mM, (c) 30 mM, and (d) 100 mM. The experimental conditions were the same as those in Figure 2. The fitted DDM model parameters were the mean deposition rate coefficient, \bar{k}_{slow} , and the fraction of the total population associated with this mode, f_{slow} . Model parameters and predictions are summarized in Table 3.

hindered or slow rate (where the mean deposition rate coefficient is defined as \bar{k}_{slow}).

Application of the DDM Model to Experimental Data. A nonlinear regression analysis (using the Levenberg–Marquardt method) was carried out to fit the DDM model (eqs 7 and 8) to the measured retained particle profiles where the merit function was given as the sum of squared residuals. Only two parameters were allowed to vary during the model optimization, the mean deposition rate coefficient, \bar{k}_{slow} , and the fraction, f_{slow} , of the total population associated with this mode. The mean deposition rate coefficient of the rapidly depositing fraction, \bar{k}_{fast} , was determined by setting the maximum deposition rate coefficient, k_{max} , equal to the transport limited rate (i.e., $\alpha_{max} = 1$), where $k_{max} = \bar{k}_{fast} + 3\sigma_{fast}$. Because this mode of the distribution takes into account the deposition of particles under *favorable* conditions, that is, those described in Figure 4a and c, it follows that the maximum value of the attachment efficiency should be 1. Under such conditions, the distribution in the particle deposition rate coefficient is assumed to be relatively narrow; thus, the standard deviation associated with this mode, σ_{fast} , was calculated as 5% of the mean, \bar{k}_{fast} . When k_{max} is equal to the particle-transport limited rate and $\sigma_{fast} = 0.05 \bar{k}_{fast}$, then the mean attachment efficiency, $\bar{\alpha}_{fast}$, is determined

to be 0.87. For the case where particles overcome an energy barrier to deposit in the primary energy well (i.e., slow deposition), a wider distribution in k is considered; thus, σ_{slow} was set equal to 15% of \bar{k}_{slow} .

Optimized model parameters (reported as $\bar{\alpha}_{slow}$ and f_{fast}) determined for the experiments conducted at 3, 10, 30, and 100 mM are presented in Table 3 (with other parameters to be discussed later). In Figure 5, the measured profiles of retained particles (symbols) are compared to predictions based on the DDM model (solid lines) as well as the classical CFT (dashed lines). This comparison indicates that the DDM model adequately captures the deposition behavior of the latex particles over the range of solution conditions investigated while requiring only two fitting parameters. As discussed earlier, the CFT fails to describe the observed particle deposition behavior under repulsive electrostatic conditions.

In the DDM model, the fraction of particles which exhibit a fast deposition rate account for the steep portion of the retained profile at the top of the column, whereas the shallow portion of the curve is described by the slow fraction. Fitted values of $\bar{\alpha}_{slow}$ become larger with increasing ionic strength, from 0.001 at 3 mM to 0.04 at 100 mM. As the salt concentration in the solution increases, the height of the repulsive energy barrier becomes smaller

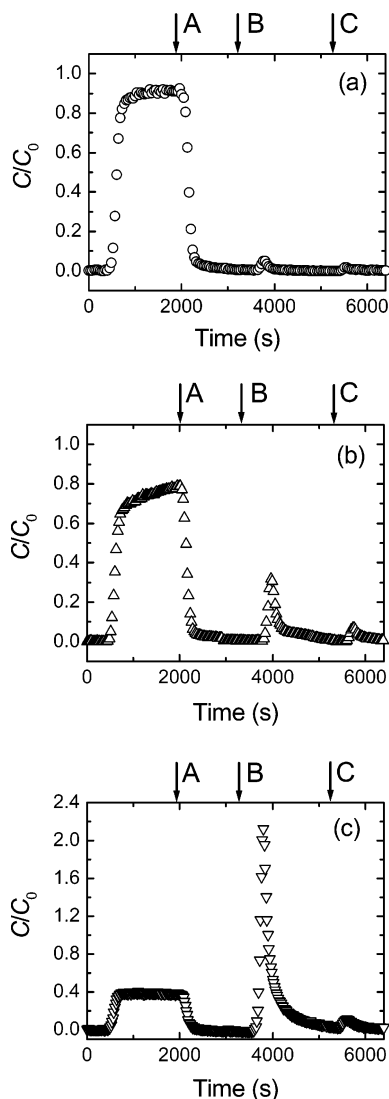


Figure 6. Representative breakthrough curves for elution experiments conducted with $3.0\ \mu\text{m}$ latex particles at different solution ionic strengths: (a) 10 mM, (b) 30 mM, and (c) 100 mM. Arrows indicate the injection of (A) a particle-free solution at the same ionic strength as that of the deposition phase (pH 8), (B) a particle-free solution at low ionic strength (0.1 mM KHCO_3), and (C) a particle-free solution at low ionic strength and high pH (1 mM KOH , pH 11). Other experimental conditions were the following: approach velocity $8.3 \times 10^{-3}\ \text{cm/s}$, porosity 0.37, mean bead diameter 0.328 mm, and temperature $20\text{--}22\ ^\circ\text{C}$.

and the efficiency of particles in overcoming this barrier is increased. The value of f_{fast} (where $f_{\text{fast}} = 1 - f_{\text{slow}}$) also becomes larger with a rise in solution ionic strength. This result can be attributed to a greater extent of favorable deposition sites with increasing ionic strength—a higher probability of encountering a deep secondary energy well and/or a near-neutrally charged surface heterogeneity. Use of eqs 6 and 8 with the optimized and calculated model parameters allows for the prediction of the normalized column effluent concentration, $C/C_{0|x=L}$ (Table 3). The results predicted by the DDM model are in excellent agreement with the measured values of $C/C_{0|x=L}$ (also included in Table 3, rightmost column). Calculated values of the adjusted coefficient of determination, R_{adj}^2 , based on the fits of the retained particle profiles further verify the validity of the DDM model in describing the observed deposition behavior.

Supporting Evidence for Dual Mode Deposition.

It has been proposed that the elution of deposited particles following exposure to a low ionic strength solution can be attributed to release from the secondary energy minimum.^{37,38,47–50} To further verify our hypothesis that the observed deviation from classical colloid filtration theory under repulsive electrostatic conditions is caused by the combined influence of fast and slow deposition, a series of elution experiments were conducted. Particles were first deposited at the ionic strength of interest followed by an equivalent injection of particle-free solution at the same ionic strength. Two additional pulses of particle-free solutions were then pumped through the column: (i) a pulse of much lower ionic strength (0.1 mM KHCO_3) to eliminate the presence of the secondary minimum and (ii) a solution at high pH (1 mM KOH) to promote release of particles deposited on metal oxide impurities.⁷

Particle breakthrough curves for elution experiments conducted at 10, 30, and 100 mM are shown in parts a, b, and c of Figure 6, respectively. The fraction of released particles, f_{rel} , was calculated for each experiment by numerically integrating the two elution pulses, N_{rel} , and dividing by the total number of particles deposited during the first phase of the experiment, N_{dep} . Values of f_{rel} are presented as a function of solution ionic strength in Table 3.

The most noteworthy result of these elution experiments is the excellent agreement between the measured values of f_{rel} and the fitted values of the parameter f_{fast} . At the two higher ionic strengths (30 and 100 mM), the quantities are nearly identical. The slightly larger difference observed at 10 mM can be attributed to the difficulty in measuring very low particle concentrations under these solution conditions.³⁷ The observed consistency between the predicted values of f_{fast} and the measured values of f_{rel} suggests that the particles eluted following injection of low ionic strength and high pH solutions are those which were retained in the secondary minimum and on bulk (metal oxide) surface impurities, where $\alpha \approx 1$. This systematic change in the degree of particle release with solution ionic strength further supports the proposed dual deposition mode model. If deposition were governed by a single mechanism whereby particles are transported over a repulsive energy barrier into a primary energy well, then an increase in the height of this barrier (under the described elution conditions) would not result in varying quantities of released particles. Similarly, if secondary minimum deposition were the sole mechanism, then elimination of this energy well would cause complete elution (release) of all retained particles (i.e., f_{rel} would approach 1 at all ionic strengths).

Conclusions

Particle deposition rates determined from the measured spatial distribution of retained particles and the suspended effluent particle concentration are in excellent agreement with the classical colloid filtration theory under favorable conditions, where deposition is controlled by the particle-transport rate. In the presence of repulsive electrostatic double-layer interactions, the concurrent existence of both favorable and unfavorable colloidal interactions results in significant deviation from the CFT. As the solution ionic strength decreases, the degree of digression between measured and predicted retained particle profiles becomes more significant. It is proposed that a fraction of the particle population exhibits slow deposition whereby particles with sufficient energy to overcome the repulsive energy barrier can reach the primary energy minimum.

The remaining particles deposit at a fast rate which is attributed to the presence of a deep secondary energy minimum and near-neutrally charged metal oxide impurities on the collector surface. The contribution of these fast deposition sites is demonstrated and measured indirectly by particle elution experiments.

A dual deposition mode model is presented which considers the combined influence of fast and slow deposition. Optimized model predictions obtained using two fitting parameters demonstrate excellent agreement with measured profiles of retained particles, suspended effluent particle concentrations, and fractions of eluted particles. Experimental data and model calculations provide evidence that the observed deviation from the classical CFT is controlled by the concurrent occurrence of both *favorable* and *unfavorable* particle deposition.

This bimodal distribution in the particle deposition rate is not apparent in the commonly measured particle breakthrough curves. Rather, the deviation from the CFT can only be observed by careful examination of the retained particle profiles. Such systematic studies conducted under well-controlled conditions are essential for identifying the key mechanisms governing particle deposition behavior.

Acknowledgment. The authors acknowledge the support of the U.S. Environmental Protection Agency (Award CR-82901001-0), the National Science Foundation (BES 0228911), and the Natural Sciences and Engineering Research Council of Canada (NSERC) for a graduate student fellowship to N.T.

Nomenclature

Symbols

A	Hamaker constant
A_S	porosity-dependent parameter of Happel's model
C	fluid-phase particle concentration
C_0	bulk (influent) particle concentration
D	hydrodynamic dispersion coefficient
d_c	diameter of spherical collector
d_p	diameter of particle
f_{fast}	fraction of population depositing at "fast" rate
f_{slow}	fraction of population depositing at "slow" rate
f_{rel}	fraction of retained particles released during elution experiment
k	particle deposition rate coefficient
k_B	Boltzmann constant, 1.3805×10^{-23} J/K
\bar{k}_{fast}	mean deposition rate coefficient associated with "fast" fraction of population
k_{fav}	deposition rate coefficient for deposition under <i>favorable</i> conditions
k_{max}	maximum (transport limited) deposition rate coefficient
\bar{k}_{slow}	mean deposition rate coefficient associated with "slow" fraction of population
L	packed length of porous medium

N_A	attraction number
N_{dep}	total number of particles deposited during column experiment
N_{eff}	number of particles in column effluent (determined by integration of breakthrough curve)
N_G	gravity number
N_{inj}	total number of particles injected into column
N_{Pe}	Peclet number
N_R	aspect ratio
N_{rel}	total number of particles released during elution phase of column experiment
N_{vdW}	van der Waals number
R_{adj}^2	adjusted coefficient of determination
S	retained particle concentration
T	absolute temperature
t	time
U	approach (superficial) velocity of fluid
v	interstitial particle velocity
x	distance along column length

Greek Symbols

α	attachment (collision) efficiency, $\alpha = \eta/\eta_0$
$\alpha_{2\text{min}}$	theoretical attachment efficiency for secondary minimum deposition based on Hahn's model
α_{BTC}	attachment efficiency determined from particle breakthrough curve
$\bar{\alpha}_{\text{fast}}$	mean attachment efficiency for "fast" fraction of population
α_{INT}	attachment efficiency calculated from intercept of retained particle profile
α_{SLOPE}	attachment efficiency calculated from slope of retained particle profile
$\bar{\alpha}_{\text{slow}}$	mean attachment efficiency for "slow" fraction of population
ϵ	porosity of a porous medium
$\Phi_{2^{\circ}\text{min}}$	depth of secondary energy minimum
η	single-collector removal efficiency, $\eta = \alpha\eta_0$
η_0	single-collector contact efficiency
μ	absolute viscosity of fluid
ρ_f	density of fluid
ρ_p	density of particle
σ_{fast}	standard deviation associated with "fast" particle deposition rate coefficient
σ_{slow}	standard deviation associated with "slow" particle deposition rate coefficient

Abbreviations

CFT	colloid filtration theory
DDM	dual deposition mode
DLVO	Derjaguin–Landau–Verwey–Overbeek
EDL	electrostatic double-layer
VDW	London–van der Waals

LA0486638